**Paper:**
Molteni, A., Masri, Z., Low, K., Yousef, H., Sienz, J. & Fraser, K. (2018). Experimental measurement and numerical modelling of dye washout for investigation of blood residence time in ventricular assist devices. *The International Journal of Artificial Organs, 41*(4), 201-212.
http://dx.doi.org/10.1177/0391398817752877

# Experimental Measurement and Numerical Modelling of Dye Washout for Investigation of Blood Residence Time in Ventricular Assist Devices

Short title: Dye Washout for Investigation of Blood Residence Time in VADs

Alessandra Molteni[1], Zubair P. H. Masri[2], Kenny W. Q. Low[3], Haitham N. Yousef[3], Johann Sienz[3], Katharine H. Fraser*[2]

[1]Calon Cardio-Technology Ltd, Institute of Life Sciences II, Swansea, SA2 8PP, United Kingdom

[2]Department of Mechanical Engineering, University of Bath, Bath, BA2 7AY, United Kingdom

[3]Advanced Sustainable Manufacturing Technologies (ASTUTE 2020) Operation, College of Engineering, Swansea University, University Bay Campus, Fabian Way, Swansea, SA1 8EN, United Kingdom

*Corresponding author: Katharine H. Fraser

Department of Mechanical Engineering, University of Bath, Bath, BA2 7AY, United Kingdom

Email: k.h.fraser@bath.ac.uk. Phone: 01225 384446

Word count: 6,234

Keywords: Ventricular Assist Devices, VADs, residence time, blood damage, shear stress, washout

**Abstract**

Ventricular Assist Devices (VADs) have become the standard therapy for end-stage heart failure. However, their use is still associated with severe adverse events related to the damage done to the blood by fluid dynamic stresses. This damage relates to both the stress magnitude and the length of time the blood is exposed to that stress. We created a dye washout technique which combines experimental and numerical approaches to measure the washout times of VADs. The technique was used to investigate washout characteristics of three commercially available and clinically used VADs: the CentriMag, HVAD and HeartMate II. The time taken to reach 5 % dye concentration at the outlet (T05) was used as an indicator of the total residence time. At a typical level of cardiac support, 5 l/min and 100 mmHg, T05 was 0.93, 0.28 and 0.16 s for CentriMag, HVAD and HeartMate II respectively and increased to 5.06, 1.64, 0.96 s for reduced cardiac support of 1 l/min. Regional variations in washout characteristics are described in the manuscript. While the volume of the flow domain plays a large role in the differences in T05 between the VADs, after standardising for VAD volume the secondary flow path was found to increase T05 by 35%. The results explain quantitatively, for the first time, why the CentriMag, which exerts low shear stress magnitude, has still been found to cause acquired von Willebrand Syndrome in patients.

## 1. Introduction

Across the world an estimated 26 million people suffer from heart failure [1]. While for the majority of patients the condition is controlled using medical therapy, and in some cases a pacemaker or implantable cardioverter defibrillator may help, those with end-stage heart failure really need a new heart. Ventricular Assist Devices (VADs) were developed to support the circulation until a suitable donor heart could be found (bridge-to-transplant), however, their success has also led to their use in patients not qualifying for a transplant (destination therapy) and are now considered gold standard treatment by some surgeons [2, 3]. The ultimate goal is heart recovery [4], although the number of patients who recover varies widely between centres, from close to 0 % to over 50 % [5, 6].

Despite their success VADs still suffer from adverse events related to the damage done to the blood such as haemolysis, platelet activation, thrombosis, bleeding and infections. Indeed, over half of all adverse events experienced by patients are related to blood trauma [7]. These complications relate both to the magnitude of the fluid dynamic stress, and the length of time the blood is exposed to that stress [8]. Designing VADs to minimise blood residence time, in addition to reducing stress, should then reduce damage. Over 5,400 VADs are now implanted annually in the USA [9] and if safer VADs are made, with fewer adverse events, an estimated 300,000 patients in the USA alone could benefit [10].

There are several methods that have the potential to be used for investigating fluid residence times in VADs. Optical techniques such as Particle Image Velocimetry and Laser Doppler Anemometry can be used to measure velocity fields [11-14]. From the velocity field, estimates of local residence times can be produced. To obtain the total residence time within a VAD it would be necessary to integrate the velocity field, for example using pathlines from the inlet to the outlet. A similar method, based on three-dimensional, three-directional, time resolved magnetic resonance phase-contrast velocity mapping, has been used for investigating blood washout in the heart [15, 16].

The most common methods for investigating washout and residence time in blood contacting devices involve the use of a tracer. The washout from the hinge region of mechanical heart valves has been investigated by optical imaging of a dairy based

colloidal suspension [17] and residence times in positive displacement VADs have been investigated similarly using methyl blue histological dye [18]. While these techniques require optical access, Francischelli *et al* [19] used a fibre optic probe inserted inside the Penn State VAD to measure local residence times. Shu *et al* [20] used three different experimental techniques to investigate washing in a dual chamber pneumatic haemodialysis pump: tracer particle visualization to investigate pathlines; dye washout to look at the overall residence time and clearance of the blood through the entire pump; and dye erosion to investigate the surface washing caused by shear stress. A similar dye washout method has also been used *in vivo*: Rovai *et al* [21] used the washout of ultrasound contrast agent to investigate blood residence in the left ventricle.

Calculating the transport of a dye through a device, by solving a scalar transport equation is another option. The first use of numerical calculations for investigating washout in blood contacting devices was by König and Clark [22] who compared their simulation of washout in a positive displacement VAD with an experiment. Goubergrits *et al* [23, 24] performed similar calculations for mechanical heart valves, summarizing their results as the time taken for the average dye concentration to reach 50 % (half dye time) and 25 % (quarter dye time) of the initial concentration.

To date there have been no published investigations of washout in rotary VADs. Since VADs are not, in general, transparent, optical methods cannot be used to look at the washout within the VAD. The aim of this work was to devise a technique to investigate both local and global washout in VADs, and use the technique to compare the washout properties of three, commonly used and commercially available, clinical VADs. Our new technique combines numerical and experimental approaches. The numerical method is based on those described above, in which a scalar transport equation is solved for the dye concentration, and therefore provides information about local washout characteristics. The experimental method uses custom optical sensors to measure dye concentration changes at the inlet and outlet of the VAD, and therefore provides global residence times. In addition, the experimental method acts as validation for the numerical calculations. The investigations revealed significant differences in the washout properties of the three VADs.

## 2. Methods

### 2.1 The Ventricular Assist Devices (VADs)

Three different commercially available VADs were investigated.

The CentriMag, CM, (Abbott Laboratories, Abbott Park, IL, formerly Thoratec Corp, Pleasanton, CA) is an extracorporeal VAD intended for short term use. It is a centrifugal pump with a magnetically levitated impeller, large clearances, and a relatively large internal volume [25]. The use of a magnetically levitated impeller creates a gap between rotating and stationary parts, resulting in a secondary flow path beneath the impeller, in which blood returns from a high pressure region near the blade tips to the lower pressure region at the centre of the impeller. Calculation of the fluid dynamic stresses showed that they are relatively low [8, 26] and hence the CM has been suggested as a benchmark for *in vitro* blood damage studies [27].

The HVAD (Medtronic, formerly HeartWare, Miami Lakes, FL) is now one of the most frequently used VADs and its small size allows implantation within the pericardium [28]. It is a centrifugal pump with a hydrodynamically and magnetically levitated impeller [29]. Like in the CM, the use of a levitated impeller creates a secondary flow path: a gap between the rotating and stationary components in which blood returns from high to low pressure. Calculation of the fluid dynamic stresses by Thamsen *et al* [30] revealed a large high stress region in the small hydrodynamic gap.

The HeartMate II, HMII, (Abbott Laboratories, Abbott Park, IL, formerly Thoratec Corp, Pleasanton, CA) has been implanted more times than any other VAD with over 20,000 implants to date [31]. It is an axial flow pump with blood washed cup-socket pivot bearings [32]. In clinical studies comparing the HMII and HVAD, the HMII had lower incidence of gastrointestinal bleeding [33], stroke [33], and fibrin-split products [34], however, in contrast the HMII had higher levels of lactate dehydrogenase (LDH) indicating higher haemolysis [34].

### 2.2 Experimental Methods

A flow rig was built to measure the washout profiles of the selected VADs. The working fluid was a mixture of glycerol (34.5 % by volume) and water which gave a viscosity of 0.00398 Pa s, as measured using a viscometer (Cannon Fenske no. 200). Dye (4 % red cochineal food colouring) was added to create the dyed fluid. As

shown in fig 1a the rig comprised: two inlet tanks, one with the dyed water-glycerol solution and the other the transparent solution; a three-way tap to switch between the inlet tanks; transparent tubing (Saint-Gobain Tygon 12.7 mm external diameter) and connections to the VADs; an outlet tank; and sensors. Custom sensors (fig 1b) were designed and built to detect the colour change in the fluid. The sensors used a white LED and photo diode positioned on opposite sides of the tubing. A custom 3D printed housing was used to hold the LED and photo diode and also to block external light from the tube. The voltage signal from the photo-diodes was recorded using LabView software at a sampling rate of 50 Hz. The voltage from the photo-diodes was calibrated to dye concentration using a series of water-glycerol samples with known dye concentration. This calibration used 3 voltage measurements at each concentration. The flow rate was measured using ultrasonic transit time flow probes (Em-tec clamp-on transducer CT3/8x1/16" A with Em-tec DIGIFLOW-EXT1) and the pressure difference between the inlet and outlet was measured using pressure transducers (Pendotech PRESS-000). The washout was first measured from dyed to colourless solution, and then from colourless to dyed solution. This process was repeated twice more to give a total of 6 individual measurements of the washout curve, for each operating condition. Since there was no significant difference between the dyed-to-colourless and colourless-to-dyed measurements the mean and standard deviation for all 6 repetitions were calculated.

### 2.3 Numerical Methods

The geometries of the flow domains of the three VADs were obtained in CAD formats: the HMII and CentriMag models were created by Fraser *et al* [8] and the HVAD model was created by Thamsen *et al* [30]. The extent of the flow domain for each VAD matched that of the actual VAD, without representing any cannulae which would be present if the VAD were implanted. To ensure fully developed flow at the entrance to the VAD, and at the outlet of the computational flow domain, straight inlet and outlet tube extensions were added.

Meshes for each of the VADs were created using a combination of ANSYS Meshing and TurboGrid (ANSYS Inc). The sizes of the meshes were: CM 4.86 million, HVAD 15.73 million, and HMII 2.52 million elements. The meshes used structured hexahedra where possible, with tetrahedra and prism layers elsewhere, and were

constructed to have a minimum of 6 elements across all gaps. The design of the HMII makes hexahedra easier to implement and most of the domain was meshed using this efficient element shape, hence the mesh size is smaller than that for the CM and HVAD. Discretization errors were assessed by comparing the results with those from calculations which used both coarser and finer meshes created with a refinement ratio of 1.26. A refinement ratio of 1.26 results in meshes with half (coarse mesh) and double (fine mesh) the number of mesh elements.

The flow equations, Navier-Stokes and scalar transport, were solved using a commercial, vertex-centered, finite volume solver ANSYS CFX (ANSYS Inc.) Transient calculations were used and the rotation of the impeller was accounted for by using sliding meshes. The length of the time step was equivalent to either $2.5^{o}$ or $5^{o}$ of rotation (for 5 l/min flow rate: CM 0.185 ms, HVAD 0.269 ms, HMII 0.035 ms) based on a preliminary time step sensitivity investigation, and with uncertainties confirmed in the mesh study reported in this work. The same refinement ratio was used for the temporal and spatial discretizations in the mesh study. The discretization schemes were set to 'high resolution' which is a blended scheme aiming for $2^{nd}$ order while avoiding overshoots.

The inlet boundary condition was mass flow rate which was fixed to give flow rates of 1, 3 or 5 l/min. The outlet boundary condition was a constant pressure of 0 Pa. The impellers were set to rotate at speeds which would give 100 mmHg pressure heads (see table 1). Blood was assumed to be a Newtonian fluid with 0.0036 Pa s viscosity (μ) and 1050 kg $m^{-3}$ density.

Reynolds numbers, Re, at the inlet were in the range 486 to 3470 which is above transition to turbulence (usually taken to occur around 2300) and in the low turbulence flow regime. However, impeller Reynolds numbers were in the range $2.10\times10^{4}$ to $6.17\times10^{4}$ so well below transition to turbulence (which occurs around $10^{6}$). Hence it can be argued that a turbulence model either should or should not be used [35]. For simplicity, in this work no turbulence model was used.

The flow calculations were run initially to establish a fully developed flow field. This was assessed by observing that the pressure head was oscillating periodically. A new scalar variable was then introduced to represent dispersion of the dye.

Molecular diffusivity was assumed to be zero and the marker concentration $[C]$ was modelled transiently as a convected scalar following the transport equation:

$$\frac{\partial [C]}{\partial t} + \nabla \cdot (u[C]) = 0 \quad (1)$$

The fluid domain was globally initialised with the dye concentration equal to 1 and the transient simulation was resumed with a concentration boundary condition of 0 at the inlet. The model was simulated until the dye concentration in the secondary flow path, or at the outlet in the HMII where there is no secondary flow path, was below 5%. The secondary flow path concentration was chosen since this often took much longer to reach 5 % than the outlet.

## 3. Results

### 3.1 Mesh Sensitivity

The influence of the discretization was assessed with a mesh refinement study. To compare the velocity fields on the different meshes the velocity at points on two perpendicular planes through the VADs was compared. The mean percentage difference in the absolute velocity at points (>50,000 individual point locations for each VAD) on the medium and fine meshes was: CM 19 %, HVAD 15 %, and HMII 34 %. The large differences are caused by small variations in the location of flow features such as a vortices, which result in relatively large differences in the pointwise velocity. Velocity fields for HMII (worst case) are shown in fig 2a.The washout curves with flow rate 5 l/min for CM, HVAD and HMII, with coarse, medium and fine meshes are shown in fig 2b. Comparing the time taken to reach 5 % dye concentration at the outlet (T05), the differences between the results from the medium meshes and either the coarse or fine meshes were all less than 5 % (mean=2.7 %).

### 3.2 Calibration of the LED-Photodiode Sensors

The calibration measurements were repeated three times and the final calibration used the mean of these three (fig 3). The largest standard deviation in the voltage occurred for the lowest dye concentration and was 0.02 V at for the inlet sensor and 0.05 V for the outlet sensor. The variation in dye concentration as a percentage, C,

with voltage signal, V, from each of the LED-photodiode sensors could be described by eqn 2:

$$C = 100\left(\frac{V - V_0}{V_{100} - V_0}\right)\left(\frac{V_{100}}{V}\right)^a \quad (2)$$

Where $V_0$ is the voltage with 0 % dye and $V_{100}$ is the voltage with 100 % dye. The exponent, *a*, was found by fitting the equation to the experimental data using Matlab (Mathworks). This exponent differed slightly (inlet: *a*=2.2, outlet: *a*=1.9) for the two sensors, due to small differences in LED-photodiode alignment (fig 3).

### 3.3 Comparison of Experimental and Numerical Washout Curves

Due to resistance in the experimental flow rig it was not possible to match all of the original numerical operating conditions. So, for the comparison between numerical and experimental results the operating conditions given in table 2 were used. For practical reasons, such as the size of the sensor housing (length=60 mm), the types of connectors between the VAD and tubing (dependent on the particular VAD), and the position of the pressure transducers, it was not possible to measure the dye washout directly at the outlet of the VADs. The location of the LED-photodiode sensor, measured from the outlet of each VAD was: CM 5 cm, HVAD 12 cm and HMII 6 cm. The dye washout curves at these locations are different from those directly at the VAD outlets: they are shifted later in time, but also have a shallower gradient as the velocity profile across the outlet tube results in an apparent spreading of the dyed fluid. So to compare numerical and experimental results washout curves, the correct downstream positions for each VAD were used. The experimental washout curves show the mean and standard deviation of 6 repetitions (fig 4). The larger standard deviations were found towards the end of the washout period; at the time when 5 % dye was reached at the outlet (T05), the standard deviation in the dye concentration was: CM 1 l/min, 2 %; CM 3 l/min, 3 %; CM 5 l/min, 3 %; HVAD 1 l/min: 5 %; and, HMII 1 l/min, 5 %. The mean of the absolute differences between experimental and numerical, outlet dye concentrations (fig 4), taken over the washout time, were within 5 %: CM 1 l/min, 2 %; CM 3 l/min, 3 %; CM 5 l/min, 5 %; HVAD 1 l/min, 1.2 %; and, HMII 1 l/min, 3 %.

### 3.4 Numerical Washout Curves at the VAD Outlets

The calculated outlet washout curves for the three VADs, at 1, 3 and 5 l/min (fig 5 a, b and c) clearly show the CM has the slowest washout and the HMII the fastest at all 3 flow rates. A comparison of the time taken to reach 5 % dye at the outlet (T05) (fig 5 d) confirms this. The CM has the largest internal volume, 28 ml from inlet to outlet in the computational domain, while the internal volumes of the HVAD and HMII are 12 and 7 ml respectively.

To eliminate the effect of VAD volume on the residence time, a type of normalization was used. The residence time of blood in a VAD can be estimated as T=V/Q, where V is the internal (priming) volume and Q is the flow rate. The time taken to reach 50 % dye at the outlet, T50, was found to be close to these T estimates: the range for all VADs, at all flow rates, was 0.76T to 0.94T. The ratio of time taken to reach 5 % dye at the outlet (T05) to T, T05/T, was around 2.0 (between 1.8 and 2.2) in the HMII, but was around 2.7 (2.6 to 2.8) in CM and HVAD (fig 5 e). The additional residence time caused by the specific flow field within the CM and HVAD is then (2.7-2.0)/2.0=0.35, so 35 %. This analysis shows that, while the volume of the VAD is a large factor accounting for the T05, after eliminating that factor the two VADs with secondary flows had T05 values which were 35 % longer than the VAD without the secondary flow. So the secondary flow significantly contributes to the residence time of the slowest portion of the fluid.

### 3.5 Washout Patterns within the VADs

The numerically calculated dye concentration patterns within the VADs were visually inspected (figs 6-8) to obtain a qualitative understanding of the regional variations in relative washout times.

CM (fig 6): Fresh fluid enters in the centre of the VAD and spreads radially, firstly along the blades, predominantly along the high pressure side at the leading edge but shifting to the low pressure side by the trailing edge. Washout from the middle of the blade passages is slower, as shown by the higher dye concentration away from the blades. The dye clearly reveals the recirculation zone downstream of the cut water at all flow rates. The original fluid lingers longest in the secondary flow, both in the central hole and the gap below the rotor. This secondary flow washout is discussed in more detail in section 3.6.

HVAD (fig 7): As in the CM, fresh fluid enters in the centre and spreads radially, again first along the high pressure side of the blade. The narrow blade passages ensure they are washed out relatively quickly. The volute and cut water are better optimised than in the CM so the fluid exits evenly at 3 and 5 l/min, without a large recirculation zone, although multiple small, transient, vortical structures of low vorticity (100-200 /s) exist downstream of the cut water at 1 l/min.

HMII (fig 8): Fluid enters past the straightener blades. These blades create vortices (strongest at 5 l/min with vorticity 6500-8500 /s) which trap the original fluid. Rotation of the impeller causes thorough mixing in that region. Downstream of the impeller the diameter of the hub reduces, with consequent increase in cross sectional area of the flow passage, causing flow separation. This recirculation zone traps the original fluid (most clearly visible at 5 l/min) leading to slow washout in this region. There is better mixing directly downstream of the diffuser blades.

### 3.6 Secondary Flow Washouts

The dye concentration remaining in the VADs, at T05, was integrated over the volume. The CM had 4.08 to 4.26 %, HVAD had 2.75 to 3.05 % and HMII had 1.90 to 2.25 % remaining. The remaining dye was mainly in the downstream part of the HMII (behind the impeller) and in the secondary flow paths of the CM and HVAD (fig 9a). Despite their very different sizes and geometries the calculated secondary flow rates for the CM and HVAD were found to be similar (fig 9b) which accounts for the similarity in their T05:T ratios. The washout of the secondary flow paths was investigated by plotting the variation in dye concentration with time at representative points within the secondary flow region (washout curves in fig 9c, locations of specific points shown in fig 9a). Due to the relatively high secondary flow rate at 1 l/min the secondary flow path washed out, either at the same rate as the outlet (CM), or faster (HVAD). However, at 5 l/min the secondary flow rate is much lower, causing a slow washout from specific portions of the secondary flow path. In the CM these regions are located in the base, which is the downstream part of the secondary flow path. In the HVAD the region is also located in the base, this time at the edge of a recirculation region.

## 4. Discussion

Our investigation has revealed there are a range of total washout times for the VADs studied. At a normal level of cardiac support, with 5 l/min flow and 100 mmHg pressure, the T05 values were 0.93 s, 0.28 s and 0.16 s with CM, HVAD and HMII respectively. For the lower flow rates, 1 and 3 l/min, which might be obtained during partial cardiac support, or during weaning, the T05 times were much longer, 5.06, 1.64, 0.96 s at 1l/min, with CM, HVAD and HMII respectively. These values should be compared with the typical time scales required for blood trauma.

Haemolysis, the process in which haemoglobin leaves the red blood cells, requires shear stress of around 150 Pa [36] which only occurs in relatively small regions of the VADs (CM 0.0067 ml, HVAD 0.029 ml, HMII 0.066 ml, in fair agreement with [8, 30]). Sublethal changes in the mechanical properties of healthy RBCs also require stresses that would only be found in small regions of the VADs: for example repeated exposures to 64 Pa for 3 s caused reductions in RBC deformability [37]. However, in the presence of oxidative stress, such as that due to heightened inflammation and free radical production associated with severe cardiovascular disease, RBCs are significantly more susceptible to shear stress [38] and thus the time scales found in this work become relevant.

The T05 times are also likely to be relevant to platelet function: a Hellums [39] type analysis of published data on platelet activation [8] shows that shear stress of around 50 Pa applied for 0.5 s should be enough for activation. The volumes of the VADs with shear stress greater than 50 Pa were CM 0.22 ml, HVAD 0.27 ml, and HMII 0.41 ml (in fair agreement with [8, 30]).

The most relevant type of blood trauma is cleavage of the high molecular weight von Willebrand factor (vWf) multimers. Increased cleavage has been reported at relatively low shear stress and exposure time combinations: 3.7 Pa for 12 s [40] and 6.5 Pa for under 0.2 s [41] or 9 Pa for the domain to unfold [42]. The volumes of the VADs with shear stress greater than 9 Pa were CM 3.1 ml, HVAD 2.0 ml, and HMII 2.0 ml (in fair agreement with [8, 30]). Cleavage of vWf is time dependant for two reasons: firstly, unravelling of the vWf molecule to expose the cleavage site is a time dependant process, and, secondly, cleavage of the vWf by the enzyme ADAMTS13 has a specific reaction rate [43]. All VADs studied to date, have been found to destroy vWf [44-49]. In VADs such as the HMII and HVAD, this can be attributed to

the high fluid stresses. In contrast, the long washout times for the CM likely explain why, although the CM, has relatively lower fluid stress magnitudes, and is considered a safe VAD, particularly in relation to RBCs [27], patients using the CM still develop acquired von Willebrand Syndrome [48].

### 4.1 Limitations

As explained in section 2.3 the Navier-Stokes equations were solved without a turbulence model. This was because Re for the impeller region were all found to be in the laminar range, and at the inlet the majority of calculations were in the laminar range. For CM at 5 l/min the inlet Re was 3470 indicating transitional flow, for which there are no good turbulence models, hence the Navier-Stokes equations were solved [35]. Turbulence has the potential to increase mixing and so reduce residence times but the effect is likely to be small for such low Re turbulence.

Blood is well known to be a multiphase, shear thinning fluid, however in this work it was treated as a single phase Newtonian fluid. The shear thinning viscosity has the potential to increase residence times by increasing the size of stagnation zones [50]. However, this effect would be small since minimal stagnation was found (section 3.5).

As described in section 3.3, the experimental setup meant it was not possible to measure dye concentration directly at the VAD outlets. This was overcome by finding the calculated dye concentrations at the experimental locations, for correct comparison. Future iterations of the rig will enable dye concentration and pressure sensors to be collocated.

## 5. Conclusions

A technique was devised for investigating both local and global washout of dye in VADs. The new technique combines a numerical method for calculating local dye concentration using a scalar transport equation, with an experimental method for determining the global washout by measuring the dye concentration at the outlet.

The technique was used to investigate the washout properties of three different VADs and significant differences in the time taken to reach 5 % dye concentration at the outlet (T05) were found. At a typical level of cardiac support, 5 l/min and 100 mmHg, T05 was 0.93, 0.28 and 0.16 s for CM, HVAD and HMII respectively and

increased to 5.06, 1.64, 0.96 s for reduced cardiac support of 1 l/min. The internal volume of the VAD was a significant factor in determining the time taken to reach 5 % dye at the outlet. However, after standardising for the VAD volume the VADs with secondary flow paths, the CM and HVAD, had T05 times which were 35 % longer than the VAD without the secondary flow path, the HMII. The results explain why the CM, which exerts low shear stress magnitude and is recognised as having low haemolysis, has still been found to cause acquired von Willebrand Syndrome in patients.

The washout calculations showed how effectively a dye can be used to highlight critical areas of the VADs with longer local residence times. The secondary flow paths are examples of such critical regions but these simulations revealed other such regions which were less intuitive and included recirculation regions in the outlet of the CM and the downstream cone-diffuser of the HMII. Our combination experimental-numerical dye washout technique will be useful in evaluating design iterations of future VADs.

**Author Contributions**

AM had the idea for the numerical simulations. ZPHM and KHF conducted the experiments. KWQL and HY conducted the numerical simulations with assistance from AM and KHF. KHF analysed the numerical and experimental data with assistance from HY. JS acquired funding for ASTUTE 2020. KHF drafted the paper and all authors contributed to revisions and agreed the final version.

**Acknowledgements**

The authors would like to thank the Biofluid Mechanics Laboratory at the Charité Universitätsmedizin Berlin for providing the CAD file for the HVAD® and Chris Moriarty and Andrew De La Bastide (Calon Cardio-Technology Ltd, Swansea, UK) and Dominica Khoo (University of Bath) for their assistance in the lab. KHF received funding from the Royal Society (RG140414). The ASTUTE 2020 (Advanced Sustainable Manufacturing Technologies) operation has been part-funded by the European Regional Development Fund through the Welsh Government and the participating Higher Education Institutions.

**Conflict of Interest**

The authors have no conflicts of interest.

## References


1. Ambrosy, A.P., et al., *The Global Health and Economic Burden of Hospitalizations for Heart Failure.* Journal of the American College of Cardiology, 2014. **63**(12): p. 1123-1133.
2. Howell, N.J. and H.S. Lim, *Ventricular assist device: destination UK*. 2015, BMJ Publishing Group Ltd and British Cardiovascular Society.
3. Westaby, S. and M. Deng, *Continuous flow blood pumps: the new gold standard for advanced heart failure?* Eur J Cardiothorac Surg, 2013. **44**(1): p. 4-8.
4. Birks, E.J., et al., *Reversal of Severe Heart Failure With a Continuous-Flow Left Ventricular Assist Device and Pharmacological Therapy.* Circulation, 2011.
5. Agarwal, R. and S. Murali, *Recovering the Broken-Hearted.* Journal of the American College of Cardiology, 2016. **68**(16): p. 1753-1755.
6. Birks, E.J., *The Promise of Recovery⁎.* JACC: Heart Failure, 2016. **4**(7): p. 577-579.
7. Kirklin, J.K., et al., *Seventh INTERMACS annual report: 15,000 patients and counting.* The Journal of Heart and Lung Transplantation, 2015. **34**(12): p. 1495-1504.
8. Fraser, K.H., et al., *A quantitative comparison of mechanical blood damage parameters in rotary ventricular assist devices: shear stress, exposure time and hemolysis index.* J Biomech Eng, 2012. **134**(8): p. 081002.
9. Kirklin, J.K., et al., *Eighth annual INTERMACS report: Special focus on framing the impact of adverse events.* The Journal of Heart and Lung Transplantation.
10. Miller, L.W. and M. Guglin, *Patient Selection for Ventricular Assist Devices.* Journal of the American College of Cardiology, 2013. **61**(12): p. 1209-1221.
11. Zhang, J., et al., *Comparison and Experimental Validation of Fluid Dynamic Numerical Models for a Clinical Ventricular Assist Device.* Artificial Organs, 2013. **37**(4): p. 380-389.
12. Zimpfer, D., et al., *Evaluation of the HeartWare ventricular assist device Lavare cycle in a particle image velocimetry model and in clinical practice.* Eur J Cardiothorac Surg, 2016. **50**(5): p. 839-848.
13. Witkowski, D., et al., *Particle image velocimetry tests on pediatric 45-cc and 30-cc ventricle assist devices: effects of heart rate on VAD operation.* Int J Artif Organs, 2017. **40**(10): p. 558-562.
14. Schule, C.Y., et al., *Turbulence measurements in an axial rotary blood pump with laser Doppler velocimetry.* Int J Artif Organs, 2017: p. 0.
15. Bolger, A.F., et al., *Transit of blood flow through the human left ventricle mapped by cardiovascular magnetic resonance.* J Cardiovasc Magn Reson, 2007. **9**(5): p. 741-7.
16. Doenst, T., et al., *Fluid-dynamic modeling of the human left ventricle: methodology and application to surgical ventricular reconstruction.* Ann Thorac Surg, 2009. **87**(4): p. 1187-95.
17. Huang Zhang, P.S., et al., *A Novel Technique for Experimental Flow Visualization of Mechanical Valves.* Asaio j, 2016. **62**(2): p. 133-8.
18. Rose, M.L., et al., *Evaluation of four blood pump geometries: the optical tracer technique.* Proc Inst Mech Eng H, 2000. **214**(4): p. 371-83.
19. Francischelli, D.E., J.M. Tarbell, and D.B. Geselowitz, *Local blood residence times in the Penn State artificial heart.* Artif Organs, 1991. **15**(3): p. 218-24.
20. Shu, F., et al., *Multimodal flow visualization and optimization of pneumatic blood pump for sorbent hemodialysis system.* Artif Organs, 2009. **33**(4): p. 334-45.
21. Rovai, D., et al., *Contrast echo washout curves from the left ventricle: application of basic principles of indicator-dilution theory and calculation of ejection fraction.* J Am Coll Cardiol, 1987. **10**(1): p. 125-34.
22. König, C.S. and C. Clark, *Flow mixing and fluid residence times in a model of a ventricular assist device.* Medical Engineering & Physics, 2001. **23**(2): p. 99-110.

23. Goubergrits, L., et al., *Numerical dye washout method as a tool for characterizing the heart valve flow: study of three standard mechanical heart valves.* Asaio j, 2008. **54**(1): p. 50-7.
24. Goubergrits, L., et al., *Characterization of an artificial valve flow using the numerical dye washout visualization technique: application to the monoleaflet valve with purged flow.* Artif Organs, 2006. **30**(8): p. 642-50.
25. Mueller, J.P., et al., *The CentriMag: a new optimized centrifugal blood pump with levitating impeller.* Heart Surg Forum, 2004. **7**(5): p. E477-80.
26. Zhang, J., et al., *Computational and Experimental Evaluation of the Fluid Dynamics and Hemocompatibility of the CentriMag Blood Pump.* Artificial Organs, 2006. **30**(3): p. 168-177.
27. Chan, C.H.H., et al., *The CentriMag Centrifugal Blood Pump as a Benchmark for In Vitro Testing of Hemocompatibility in Implantable Ventricular Assist Devices.* Artificial Organs, 2015. **39**(2): p. 93-101.
28. Wieselthaler, G.M., et al., *Initial clinical experience with a novel left ventricular assist device with a magnetically levitated rotor in a multi-institutional trial.* J Heart Lung Transplant, 2010. **29**(11): p. 1218-25.
29. Larose, J.A., et al., *Design concepts and principle of operation of the HeartWare ventricular assist system.* Asaio j, 2010. **56**(4): p. 285-9.
30. Thamsen, B., et al., *Numerical Analysis of Blood Damage Potential of the HeartMate II and HeartWare HVAD Rotary Blood Pumps.* Artif Organs, 2015. **39**(8): p. 651-9.
31. Shekar, K., S.D. Gregory, and J.F. Fraser, *Mechanical circulatory support in the new era: an overview.* Critical Care, 2016. **20**(1): p. 66.
32. Griffith, B.P., et al., *HeartMate II left ventricular assist system: from concept to first clinical use.* The Annals of Thoracic Surgery, 2001. **71**(3): p. S116-S120.
33. Lalonde, S.D., et al., *Clinical differences between continuous flow ventricular assist devices: a comparison between HeartMate II and HeartWare HVAD.* J Card Surg, 2013. **28**(5): p. 604-10.
34. Birschmann, I., et al., *Ambient hemolysis and activation of coagulation is different between HeartMate II and HeartWare left ventricular assist devices.* J Heart Lung Transplant, 2014. **33**(1): p. 80-7.
35. Fraser, K.H., et al., *The use of computational fluid dynamics in the development of ventricular assist devices.* Med Eng Phys, 2011. **33**(3): p. 263-80.
36. Zhang, T., et al., *Study of flow-induced hemolysis using novel Couette-type blood-shearing devices.* Artif Organs, 2011. **35**(12): p. 1180-6.
37. McNamee, A.P., et al., *Biphasic impairment of erythrocyte deformability in response to repeated, short duration exposures of supraphysiological, subhaemolytic shear stress.* Biorheology, 2016. **53**(3-4): p. 137-149.
38. McNamee, A.P., et al., *Oxidative Stress Increases Susceptibility of Red Blood cells to Shear-Mediated Damage.* International Journal of Artificial Organs, 2017. **40**(8): p. 435.
39. Hellums, J.D., *1993 Whitaker lecture: Biorheology in thrombosis research.* Annals of Biomedical Engineering, 1994. **22**(5): p. 445-455.
40. Tsai, H.M., Sussman, II, and R.L. Nagel, *Shear stress enhances the proteolysis of von Willebrand factor in normal plasma.* Blood, 1994. **83**(8): p. 2171-9.
41. Vincentelli , A., et al., *Acquired von Willebrand Syndrome in Aortic Stenosis.* New England Journal of Medicine, 2003. **349**(4): p. 343-349.
42. Di Stasio, E. and R. De Cristofaro, *The effect of shear stress on protein conformation: Physical forces operating on biochemical systems: The case of von Willebrand factor.* Biophysical Chemistry, 2010. **153**(1): p. 1-8.
43. Zhang, X., et al., *Mechanoenzymatic cleavage of the ultralarge vascular protein von Willebrand factor.* Science, 2009. **324**(5932): p. 1330-4.
44. Goda, M., et al., *Time course of acquired von Willebrand disease associated with two types of continuous-flow left ventricular assist devices: HeartMate II and CircuLite Synergy Pocket Micro-pump.* J Heart Lung Transplant, 2013. **32**(5): p. 539-45.

45. Crow, S., et al., *Comparative analysis of von Willebrand factor profiles in pulsatile and continuous left ventricular assist device recipients.* Asaio j, 2010. **56**(5): p. 441-5.
46. Heilmann, C., et al., *Acquired Von Willebrand syndrome is an early-onset problem in ventricular assist device patients☆,☆☆.* European Journal of Cardio-Thoracic Surgery, 2011. **40**(6): p. 1328-1333.
47. Meyer, A.L., et al., *Acquired von Willebrand syndrome in patients with a centrifugal or axial continuous flow left ventricular assist device.* JACC Heart Fail, 2014. **2**(2): p. 141-5.
48. Morrison, K.A., et al., *Acquired von Willebrand Disease During CentriMag Support Is Associated with High Prevalence of Bleeding During Support and After Transition to Heart Replacement Therapy.* ASAIO Journal, 2014. **60**(2): p. 241-242.
49. Coutance, G., et al., *Acquired von Willebrand disease in Jarvik 2000 recipients: A single center experience.* International Journal of Cardiology, 2012. **159**(1): p. 57-58.
50. Fraser, K.H., et al., *Computational fluid dynamics analysis of thrombosis potential in left ventricular assist device drainage cannulae.* Asaio j, 2010. **56**(3): p. 157-63.

Tables

Table 1

VAD operating conditions for the numerical calculations of dye washout (used for all sections excluding 3.3)

| VAD | flow rate (l/min) | rotational speed (rpm) |
|---|---|---|
| CentriMag (CM) | 1 | 2150 |
| | 3 | 2200 |
| | 5 | 2250 |
| HVAD | 1 | 2800 |
| | 3 | 2900 |
| | 5 | 3100 |
| HeartMate II (HMII) | 1 | 9550 |
| | 3 | 10700 |
| | 5 | 12000 |

Table 2

VAD operating conditions for comparison of numerical and experimental washout results. Numerical pressure head is the mean and standard deviation of the last 10 impeller rotations. Experimental pressure head and flow rate are the mean and standard deviation of the 6 repetitions. (Used for section 3.3).

| VAD | rotational speed (rpm) | Numerical | | Experimental | |
|---|---|---|---|---|---|
| | | flow rate (l/min) | pressure (mmHg) | flow rate (l/min) | pressure (mmHg) |
| CentriMag (CM) | 2150 | 1 | 101 +/- 1 | 1.02 +/- 0.002 | 101 +/- 1 |
| | 2200 | 3 | 100 +/- 1 | 2.81 +/- 0.22 | 99.7 +/- 5 |
| | 3150 | 5 | 212 +/- 2 | 4.58 +/- 0.14 | 176 +/- 8 |
| HVAD | 2800 | 1 | 103 +/- 4 | 0.98 +/- 0.11 | 102 +/- 2 |
| HeartMate II (HMII) | 6240 | 1 | 39 +/- 1 | 0.96 +/- 0.04 | 43.4 +/- 6 |

Figure captions

Figure 1: (a) Experimental flow rig consisting of two inlet tanks with clear and dyed glycerol-water, a three-way tap, VAD, outlet tank, pressure transducers, flow meter and custom made LED-photo diode sensors. (b) Detailed view of the custom made LED-photo diode sensors. The LED is located at position ‘a’ and photo-diode at positon ‘b’. The 3D printed housing holds the components on opposing sides of the transparent tubing and blocks external light.

Figure 2: (a) Velocity fields in the HMII with coarse, medium and fine meshes, as an example of the influence of the mesh on the local velocity. (b) Comparison of the numerical dye washout curves at the outlets of the three VADs at 5 l/min, using coarse (- - -) medium (-----) and fine (. . . .) meshes.

Figure 3: The calibration curves for the inlet and outlet LED-photo diode sensors. Experimental mean of 3 repeats, error bars show standard deviation.

Figure 4: Comparison of numerical (-----) and experimental mean (- - -) +/- standard deviation (. . . .) dye washout curves for the (a) CM, (b) HVAD and (c) HMII. Operating conditions are given in table 2. Experimental mean and standard deviation of 6 repeats.

Figure 5: Numerical dye washout curves at the outlets of the three VADs at (a) 1 l/min, (b) 3 l/min and (c) 5 l/min. (d) Time taken to reach 5 % dye concentration at the VAD outlet (T05).

Figure 6: Variation in dye concentration within the CM for 1, 3, and 5 l/min, at 80 % and 40 % dye concentration at the outlet. Velocity vectors (relative to the moving frame) are also shown.

Figure 7: Variation in dye concentration within the HVAD for 1, 3, and 5 l/min, at 80 % and 40 % dye concentration at the outlet. Velocity vectors (relative to the moving frame) are also shown.

Figure 8: Variation in dye concentration within the HMII for 1, 3, and 5 l/min, at 80 % and 40 % dye concentration at the outlet. Velocity vectors (relative to the moving frame) are also shown.

Figure 9: Washout of the secondary flow paths. (a) Dye concentration in the secondary flow paths of the CM and HVAD at 1 and 5 l/min at the time corresponding to 20 % dye concentration at the outlet. The cross section is identical to that in the lower half of figures (7) and (8) but focussed in on the secondary flow path. (b) Secondary flow rates for the CM and HVAD. (c) Dye washout curves at specific locations within the secondary flow paths. Location points are shown in (a).

Figure 1

a

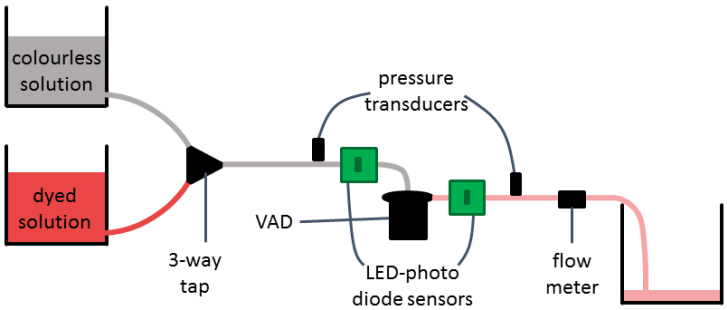
colourless solution
dyed solution
3-way tap
pressure transducers
VAD
LED-photo diode sensors
flow meter

b

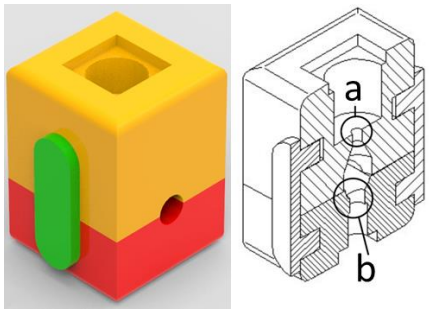
a
b

Figure 2

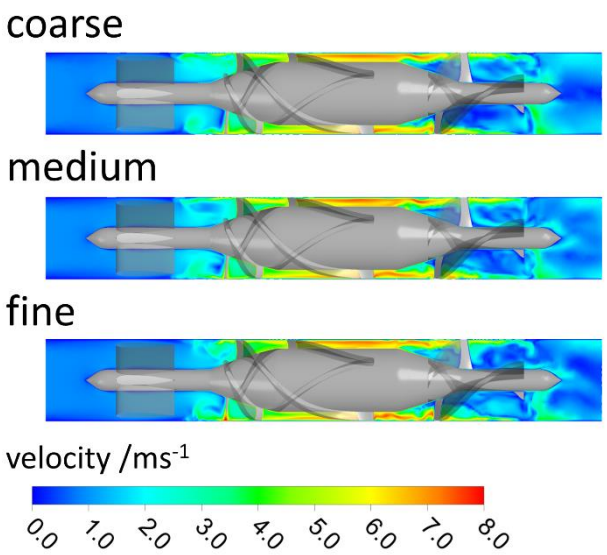
coarse
medium
fine
velocity /ms-1
0.0
1.0
2.0
3.0
4.0
5.0
6.0
7.0
8.0

a

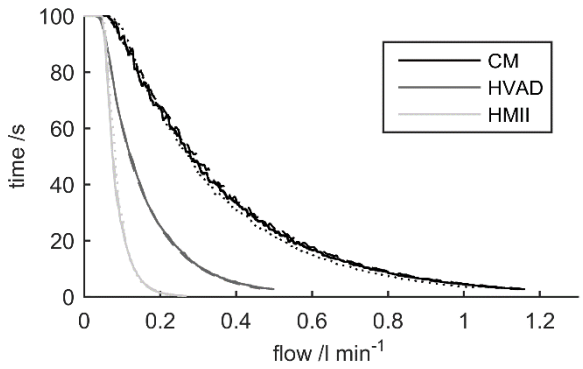
100
80
60
40
20
0
time /s
0
0.2
0.4
0.6
0.8
1
1.2
flow /l min-1
CM
HVAD
HMII

b

Figure 3

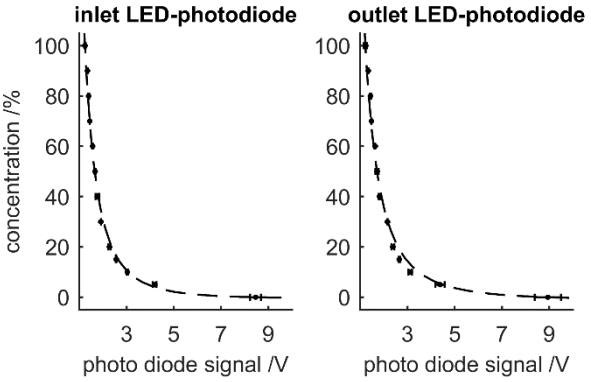
inlet LED-photodiode
outlet LED-photodiode
concentration /%
100
80
60
40
20
0
3
5
7
9
photo diode signal /V

Figure 4

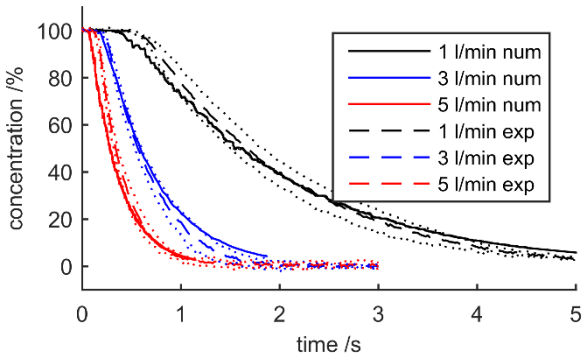
concentration /%
time /s
1 l/min num
3 l/min num
5 l/min num
1 l/min exp
3 l/min exp
5 l/min exp

a

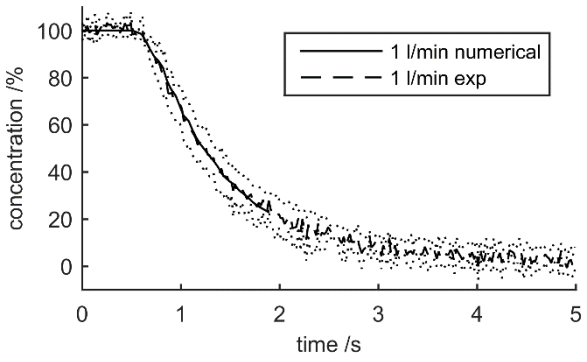
concentration /%
time /s
1 l/min numerical
1 l/min exp

b

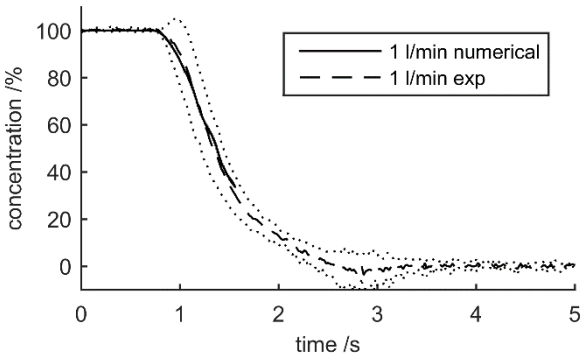
concentration /%
time /s
1 l/min numerical
1 l/min exp

c

Figure 5

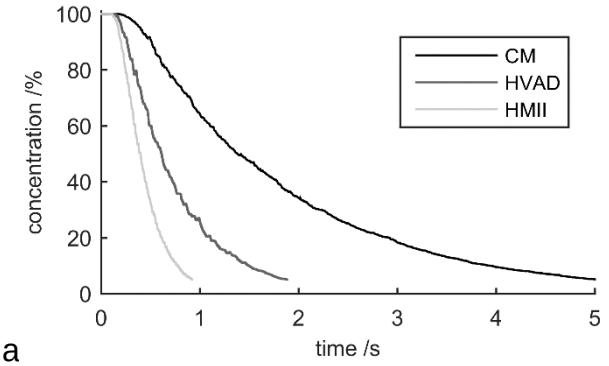


a

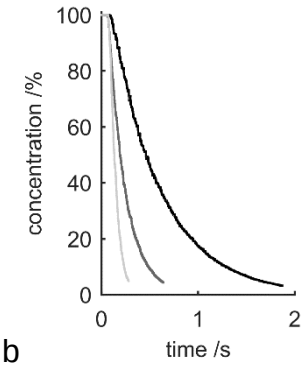


b

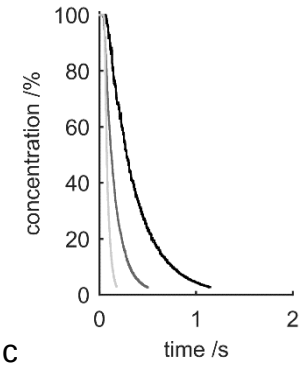


c

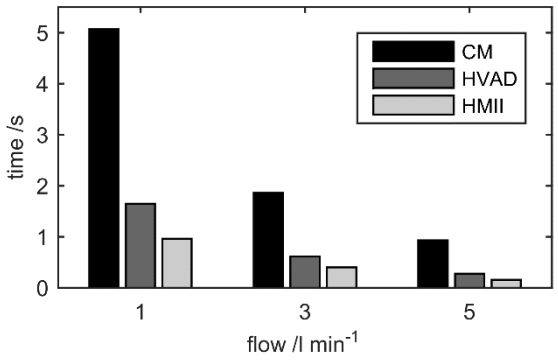


d

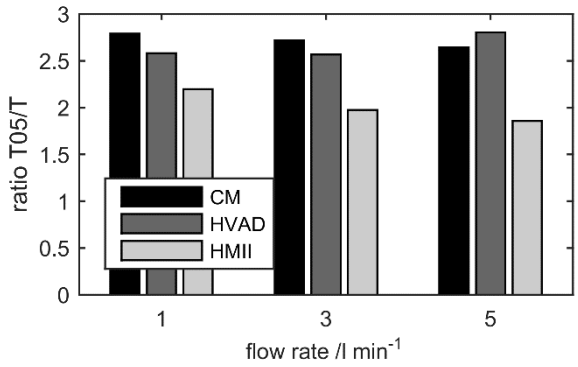


e

Figure 6

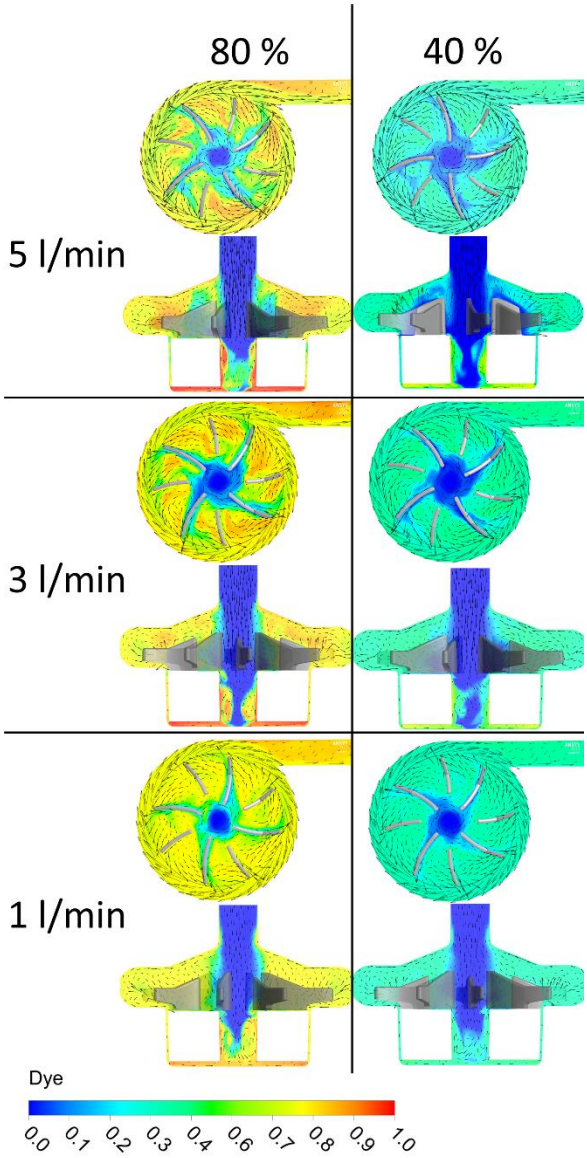

Figure 7

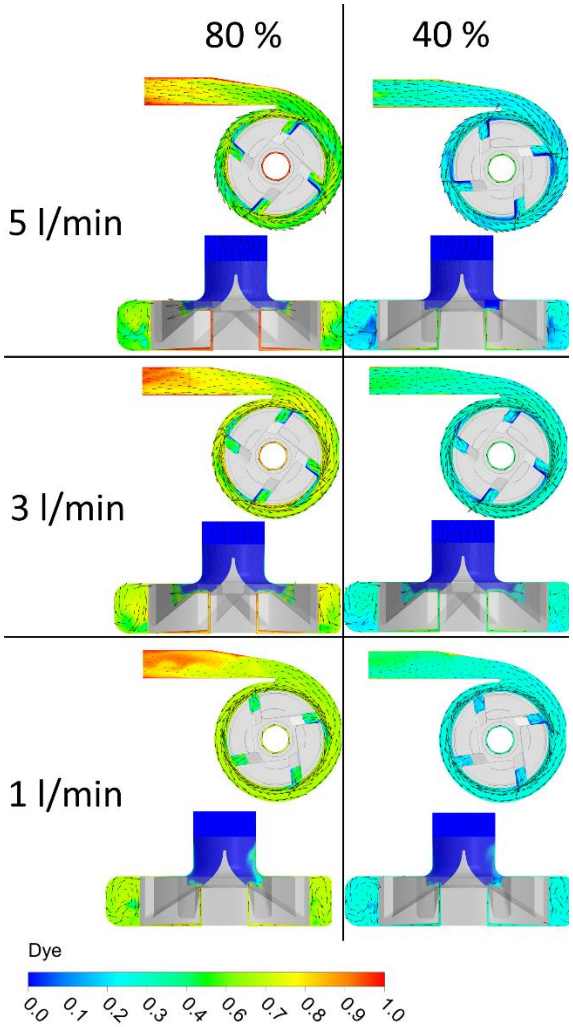

Figure 8

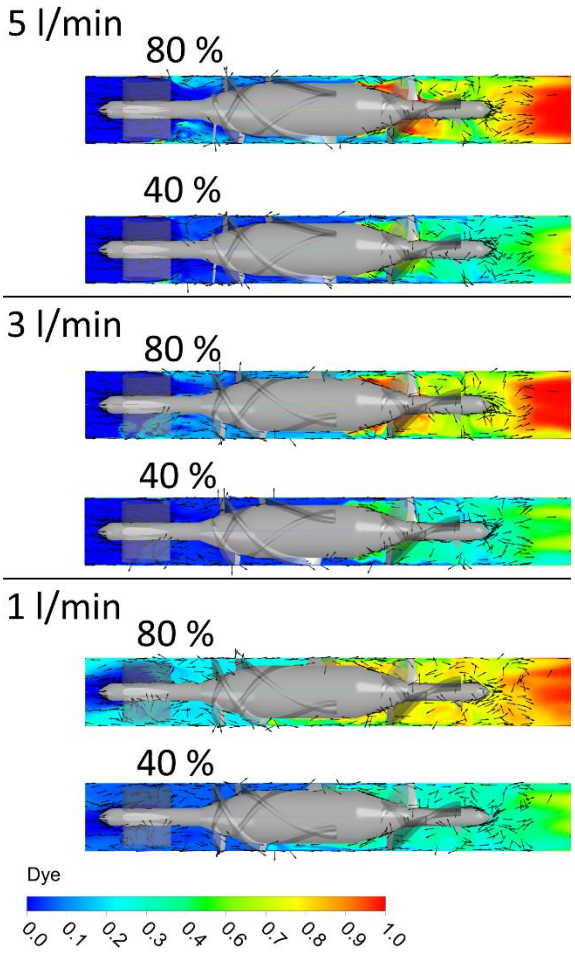
5 l/min
80 %
40 %
3 l/min
80 %
40 %
1 l/min
80 %
40 %
Dye
0.0 0.1 0.2 0.3 0.4 0.6 0.7 0.8 0.9 1.0

Figure 9

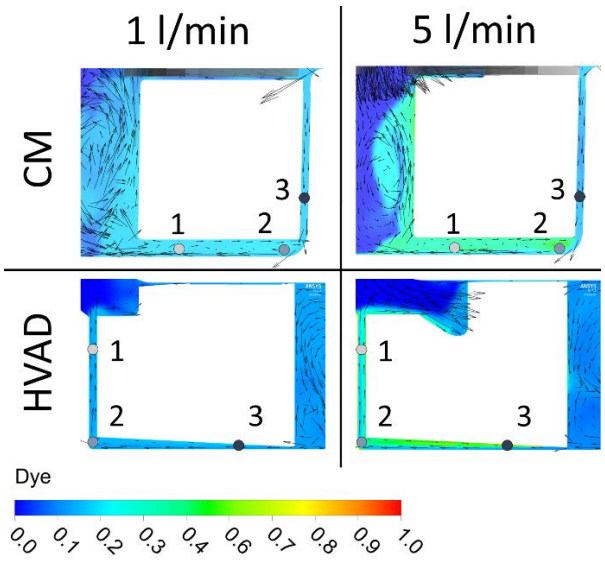
1 l/min
5 l/min
CM
HVAD
1
2
3
Dye
0.0 0.1 0.2 0.3 0.4 0.6 0.7 0.8 0.9 1.0

a

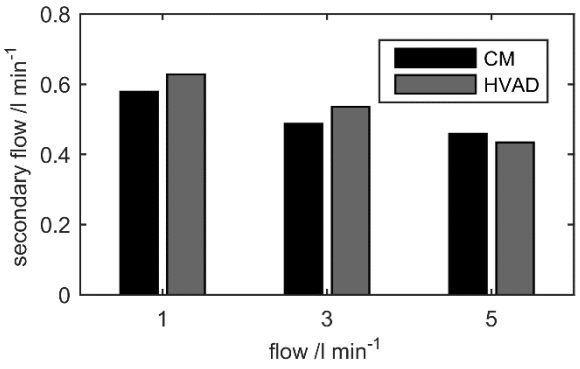
secondary flow /l min-1
flow /l min-1
CM
HVAD
0
0.2
0.4
0.6
0.8
1
3
5

b

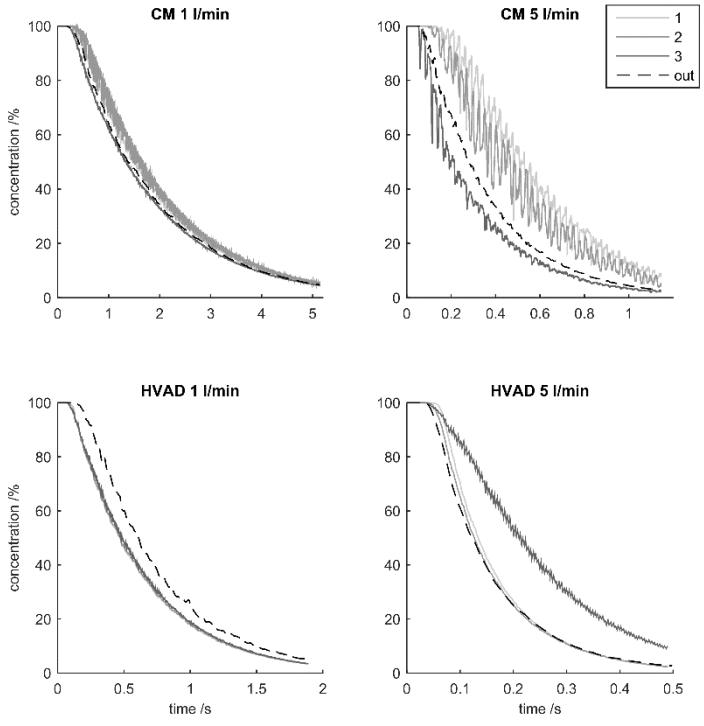
CM 1 l/min
CM 5 l/min
HVAD 1 l/min
HVAD 5 l/min
concentration /%
time /s
1
2
3
out

c